RSC Advances

PAPER

View Article Online
View Journal | View Issue

Cite this: *RSC Adv.*, 2023, **13**, 8765

Rapid and efficient removal of multiple aqueous pesticides by one-step construction boric acid modified biochar†

Niannian Cao,[a] Jiawen Ji,[a] Changsheng Li,[a] Meng Yuan,[a] Xuanjun Guo,[a] Xingxing Zong,[b] Liqin Li,[b] Yongqiang Ma,[a] Chen Wang*[b] and Sen Pang*[a]

Tricyclazole, propiconazole, imidacloprid, and thiamethoxam are commonly used pesticides in paddy fields. It is necessary and practical to remove pesticides from the water environment because the low utilization rate of pesticides will produce residues in the water environment. It is known that there are few studies on the preparation of biochar adsorption pesticides by the walnut shell and few studies on the removal of tricyclazole and propiconazole. Based on this, this paper used the walnut shell as raw material and boric acid as an activator to prepare biochar by the one-step method. The boric acid modified walnut shell biochar (WAB4) with a specific surface area of 640.6 $m^2\ g^{-1}$, exhibited the high adsorption capacity of all four pesticides (>70%) at pH 3–9. The adsorption capacities of tricyclazole, propiconazole, imidacloprid, and thiamethoxam were 171.67, 112.27, 156.40, and 137.46 mg g^{-1}, respectively. The adsorption kinetics fitted the pseudo-second-order kinetic model and the adsorption isotherm curves conformed to the Freundlich isotherm model. The adsorption of pesticides by WAB4 was associated with hydrogen bonding, pore filling, hydrophobic effects, and π–π interactions. More significantly, WAB4 has excellent adsorption capacity compared to other adsorbents for real water samples. Finally, walnut shell biochar has no significant acute toxicity to *Daphnia magna*. This work shows that walnut shell-based biochar has a good effect on the removal of pesticides at a wide range of pH and is economical and safe, providing a new idea for the removal of pesticides in water.

Received 2nd December 2022
Accepted 3rd March 2023

DOI: 10.1039/d2ra07684e

rsc.li/rsc-advances

1. Introduction

Oryza sativa L. is one of the main crops of agriculture and one of the main foodstuffs for the world's population.[1] To ensure rice production can cope with population growth, pesticides play an important role in rice growth. Tricyclazole and propiconazole are commonly used in rice paddy fields as fungicides[2] to prevent *Pyricularia oryzae* and *Rhizoctonia solani*.[3,4] Imidacloprid and thiamethoxam mainly prevent rice pests *Nilaparvata lugens*, *Sogatella furcifera*, and *Laodelphax striatellus*.[5] These four pesticides are frequently detected in the environment due to their higher water solubility, migration, and good flowability.[6–9] Tricyclazole (1.20 μg L^{-1}) and propiconazole (0.291–1.15 μg L^{-1}) were frequently detected in surface water.[10,11] Some studies have detected neonicotinoids in groundwater, with maximum concentrations of imidacloprid of 1.93 μg L^{-1} and thiamethoxam of 8.93 μg L^{-1}.[7] Tricyclazole is persistent in paddy soil, which may cause potential risks to nearby natural water sources.[12,13] Propiconazole has a half-life of 101–336 days[14] and exhibits relatively high toxicity to a variety of aquatic organisms.[15] It was found that tricyclazole caused carbohydrate and lipid metabolism disorder and hepatocyte apoptosis in zebrafish liver.[16] The detection of pesticides in the aquatic environment may have adverse effects on aquatic organisms and humans. Thus, it is necessary and important to remove pesticides from water.

Currently, the main methods for the removal of pesticides from the environment include photocatalysis, advanced oxidation process (AOPs), bioremediation, and adsorption.[17,18] Because of its low cost, abundant resources, and organic functional groups, biochar is a widely used adsorption material in current adsorption methods.[19–21] The main methods of biochar preparation include pyrolysis, gasification, and hydrothermal carbonization (HTC).[22] Most of the current biochar adsorbents have a long adsorption time (ranging from a few hours to tens of days) and a large amount of adsorbent, so it is necessary to develop new adsorbents with fast adsorption, easy regeneration, and environmental friendliness. The adsorption capacity of biochar without modification by simple pyrolysis is low, which can be overcome by adding the functionalized groups through modification. Boric acid is a novel low-toxicity activation

[a]*Department of Applied Chemistry, College of Science, China Agricultural University, Beijing, 100193, China. E-mail: pangsen7812@cau.edu.cn*

[b]*State Key Laboratory of NBC Protection for Civilians, Beijing, 102205, China. E-mail: wangchenpla@163.com*

† Electronic supplementary information (ESI) available. See DOI: https://doi.org/10.1039/d2ra07684e

reagent.[23] At the moment, boric acid modified biochar has been proven to remove antibiotics and sulfamethoxazole from water.[23–25] The material prepared by metal–organic skeleton-cyclodextrin adsorbed and removed nicotinoid pesticides, and the adsorption capacity of thiamethoxam was 2.88 mg g^{-1}.[26] According to statistics, there have been few studies on the adsorption of tricyclazole and propiconazole by biochar in recent years, with a poor adsorption effect and a hazy adsorption capacity.[27]

In recent years, various plant-based wastes have been recognized as effective adsorbents to replace activated carbon. The annual output of walnut (with shell) in the world is about 2 million tons,[28] of which the walnut shell is an easily neglected waste[29] with the advantage of large volume and low cost.[30] Walnut shell is a lignocellulosic agricultural waste composed of cellulose (17.74%), hemicellulose (36.06%), and lignin (36.90%).[31] Because the walnut shell has a high lignin content and the adsorption functional groups primarily include carboxyl and phenolic hydroxyl groups, it is an ideal material for biochar preparation. The walnut shell has been widely used in adsorption studies of heavy metals[32] and antibiotics.[33] Few studies use the boric acid-modified walnut shell for pesticide adsorption.

In this study, to solve the problems of low adsorption capacity, complex preparation process, and high cost, we selected agricultural waste walnut shell as a raw material, modified with boric acid, to prepare novel biochar in one-step and to investigate the potential for pesticide removal in water. The specific objectives were to: (1) characterization of the prepared biochar materials mainly including specific surface area, porosity, elemental composition, and morphological characteristics; (2) investigate the effects of pH, contact time, and initial concentration of pesticides on the removal of pesticides by modified biochar; (3) investigate the possible adsorption mechanisms of biochar on selected pesticides; (4) compare with other adsorbents, examine the regeneration capacity and the adsorption capacity of real water samples; (5) assessing the safety of biochar materials.

2. Material and methods

2.1. Materials and reagents

The chemical reagents in this paper were all of the analytical grades. Several pesticides: tricyclazole (98%), propiconazole (98%), imidacloprid (95%), and thiamethoxam (98%) were purchased from Aladdin Chemistry Co. Ltd. The walnut shell was obtained from the local market. Boric acid (H_3BO_3, 99.8%) and formic acid (99%) were purchased from Shanghai Macklin Biochemical Co., Ltd. HPLC grade acetonitrile was purchased from Thermo Fisher Scientific. Ultrapure water (18.2 MΩ cm^{-1}) produced on a Milli-Q purification system was used throughout the experiment.

2.2. Preparation of walnut shell biochar and modification

The walnut shell was sieved through a 100-mesh sieve and then used. Walnut shell powder (2 g), impregnated with boric acid (0.5 M) in a solid–liquid ratio set at 1 : 0, 1 : 0.5, 1 : 1, 1 : 2, 1 : 4, was placed in a covered crucible in the central area of the muffle furnace. The crucible was first heated to 600 °C at a heating rate of 10 °C min^{-1} and kept at 600 °C for 2 h, and then cooled naturally. The resulting product was ground uniformly, washed with water, dried in a lyophilizer, and prepared for use. The resulting materials were labeled WA, WAB0.5, WAB1, WAB2, and WAB4.

2.3. Characterizations of adsorbents

The composition and morphology of adsorbents were characterized by scanning electron microscopy (SEM, Quanta FEG 250, FEI Company, Hillsboro, USA). The Specific surface area (SSAs), pore volumes (PVs), and pore size of the products were determined using 3H-2000PS2 (Beishide Instrument, China). The sample was degassed at 120 °C for 3 h before determination. Brunauer–Emmett–Teller (BET) method was used to calculate the specific surface area of activated carbon, and Barrett–Joyner–Halenda (BJH) method was used to calculate the pore size distribution. Raman spectroscopy was used to determine the carbon defects and graphitization of the modified biochar (DXR2 Raman microscope, Thermo Fisher Scientific, USA). Surface functional groups of adsorbents were analyzed by Fourier-transform infrared spectroscopy (FTIR) on a PerkinElmer instrument (Massachusetts, USA) within the 4000–450 cm^{-1} region (KBr pellets). The zeta potentials of the adsorbents were measured by Zetasizer Nano ZS90 (Malvern Panalytical company, Britain). X-ray photoelectron spectroscopy (XPS) was used to probe the surface chemistry and chemical states. All binding energies were calibrated with C 1s at 284.8 eV. The elemental compositions including C, H, O, N, and B contents of the adsorbents were measured using an organic element analyzer (Elementar Vario EL cube, Germany) and an ICP analyzer (Thermo ICP-OES 7200, USA).

2.4. Adsorption experiments

The sorbent screening experiments were carried out in 10 mL of a system containing four 2 mg L^{-1} pesticide mixtures at 0.5 g L^{-1} sorbent, pH = 7 and T = 298 K. Adsorption kinetics experiments were carried out with four pesticide solutions of 5 mg L^{-1} at 298 K. The amount of WAB4 was 1 g L^{-1}, pH = 7, and the adsorption time was 0–30 min. Adsorption isotherm experiments were carried out using WAB4 (1 g L^{-1}) on tricyclazole (1–500 mg L^{-1}), propiconazole (1–150 mg L^{-1}), imidacloprid (1–500 mg L^{-1}), and thiamethoxam (1–400 mg L^{-1}), respectively. The temperatures were set at 298 K, 308 K, and 318 K and shaken at 170 rpm for 2 h until equilibrium was reached. After the adsorption was completed, the carbon material was separated by a centrifuge, passed through a microfiltration membrane (13 mm × 0.22 μm) to obtain a residual solution, and then the residual pesticide was quantitatively analyzed.

2.5. Regeneration experiments

The desorption and regeneration performance of adsorbent is very important in the application process. The concentration of WAB4 was 1 g L^{-1} according to the above optimized conditions. The aqueous solution of four pesticides mixed with 5 mg L^{-1} was prepared with pure water with pH = 7. Five adsorption–

desorption cycles were performed. In each cycle, the adsorbed pesticide was washed with acetonitrile and re-dried for use.

2.6. Experiment on risk evaluation of aquatic organisms *Daphnia magna*

Daphnia magna is a model species sensitive to environmental change in the aquatic environment and is frequently used to assess pollutant toxicity.[34] The safety assessment of biochar can be evaluated using the *Daphnia magna* acute toxicity test. The acute toxicity test was designed under Organisation for Economic Cooperation and Development (OECD) guideline 202.[35] Five concentrations of 1, 10, 50, 100, and 200 mg L^{-1} were selected for the experiment according to the guidelines and limited experimental concentration, and blank control was set at the same time. Oxygen-saturated water of 30 mL was added to a 50 mL beaker, oxygen-saturated water of 30 mL was added to a 50 mL beaker, and homogenized samples ($n = 20$) were born for 6–24 h were selected. The light cycle was maintained at 16 h light: 8 h dark and a temperature of 21 ± 1 °C.[36] Inhibition and death at 24 and 48 h were then observed.

2.7. Analytical methods

The concentrations of the four pesticides were determined using liquid chromatography-tandem mass spectrometry (LC-MS/MS, Agilent 6410B). The mobile phase was acetonitrile and formic acid water (0.1%) in a volume ratio of 70 : 30, with a flow rate of 0.2 mL min^{-1} and a column temperature of 25 °C. The chromatographic column was an Athena C18-WP (2.1 × 50 mm, 3 μm). The injection volume for one sample was 5 μL. Quantitative analysis was performed under an electrospray positive ion source (ESI+) and multiple reaction monitoring mode (MRM). Specific MRM parameters for the four pesticides are shown in Table S1 and Fig. S1.†

3. Results and discussions

3.1. Physiochemical characterization of the biochar

3.1.1. Elemental analysis. Elemental analysis was performed on all biochars to obtain their chemical compositions and the corresponding contents of each component. Table S2† summarizes the types and contents of the elements. The unmodified biochar is dominated by the C element, and the content of B, H, and O elements in the modified biochar increases with the increase of the boric acid aqueous solution ratio, indicating that the boric acid aqueous solution can improve the elemental composition of the biochar surface. The O content in the biochar was all greater than 10%, and the H/C, O/C and N/C molar ratios were all higher than those of the unmodified biochar because the carbon content decreased and the oxygen content increased after boric acid modification. This method of boric acid modification increases the content of oxygen in biochar, some oxygen atoms were stored in the modified biochar in the form of oxygen-containing functional groups.[30] The results of H/C, O/C, and N/C showed that the degree of carbonization decreased after modification, which was consistent with the later Raman spectroscopy results. WAB4 has the highest oxygen content, which is consistent with the FTIR and XPS results. Simultaneously, the content of element B after activation is not high, which may be due to the low content of boron in the boric acid solution.

3.1.2. Surface morphology of biochars. SEM analyses were performed to determine morphological differences between WA and WAB4. As shown in Fig. 1, WA is directly carbonized with a smooth surface, whereas WAB4 after boric acid activation is rich in pores and contains a porous structure. The formation of pores is attributed to the pyrolysis of boric acid at high temperatures to produce boron trioxide and water, which forms pores when the water evaporates.[37,38]

3.1.3. Specific surface area and pore size distribution. The main physical properties that affect biochar adsorption capacity are porosity and specific surface area.[39] Fig. 2a shows the nitrogen adsorption–desorption isotherms at 77 K. WA and WAB0.5 show microporous structures with relatively small outer surface microporous volumes with reversible type I isotherms, and adsorption quickly reaches saturation. The isotherms of WAB1, WAB2, and WAB4 also show typical type I isotherms without obvious hysteresis loops, indicating that the modified biochar is dominated by microporous structures.[40–42] The specific surface area and pore size of all biochar were measured, and the results are shown in Table 1. In the preparation process of WA, high-temperature carbonization will form a part of ash,[43] which will not be fully converted into biochar. Thus, it is essential to activate the raw materials. The specific surface area of raw materials is only 1.44 m^2 g^{-1}, and the pristine biochar carbonized at 600 °C reached 436.29 m^2 g^{-1}. With the addition of 0.5 M boric acid content, the specific surface area of the modified biochar increased. The largest was WAB4 with a specific surface area of 640.6 m^2 g^{-1} and 89.6% of micropores. Improved specific surface area and pore volume are known to enhance the adsorption of organic pollutants on biochar.[42,44] As the aqueous solution of boric acid increases, more gases (*e.g.*, HBO_2, B_2H_6, and H_2O) are produced during the pyrolysis process, while at higher temperatures, evaporation produces more pores, promoting the generation and formation of porous structures, with a consequent increase in S_{BET}.[45,46] Thus, the aqueous boric acid solution increases the specific surface area and porosity of the biochar.

3.1.4. Chemical surface characterization. In the Raman spectrum of the biochar in Fig. 2c, two characteristic bands are located at approximately 1350 cm^{-1} (D band) and 1590 cm^{-1} (G band).[47,48] The G band may be the graphite structure of sp^2 or is alkene C=C. The D band points to the presence of defective and unsaturated carbon atoms.[39] As the ratio of boric acid aqueous solution increases, I_D/I_G increases, and the disordered structure of biochar increases. The increase of oxygen-containing functional groups during the modification process is an impetuous reason for the increase of amorphous carbon.

The FTIR spectrum of WA, WAB0.5, WAB1, WAB2, and WAB4 are depicted in Fig. 2d. The peak at 3300 cm^{-1} was ascribed as –OH (alcoholic and phenolic) stretching. The wave number 2322 cm^{-1} was attributed to the stretching vibration of the C≡C[49] or the C≡N stretching,[40] which is verified by the results of elemental analysis. Wave number 1921 cm^{-1} was the

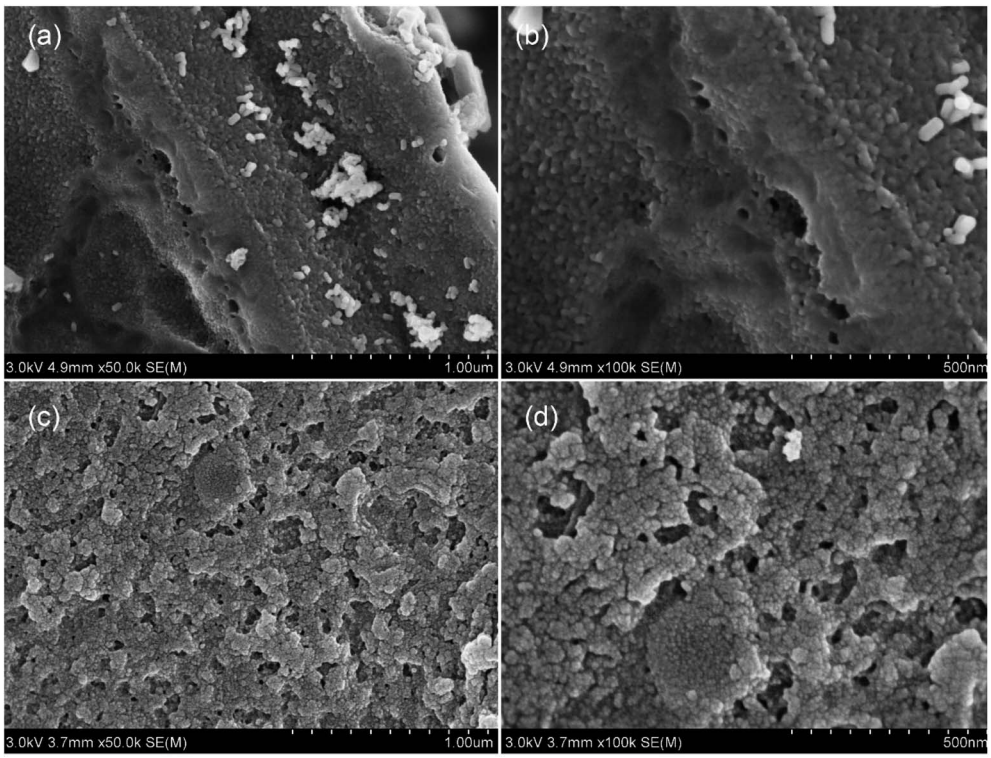

Fig. 1 SEM images of pristine WA (a and b) and WAB4 (c and d).

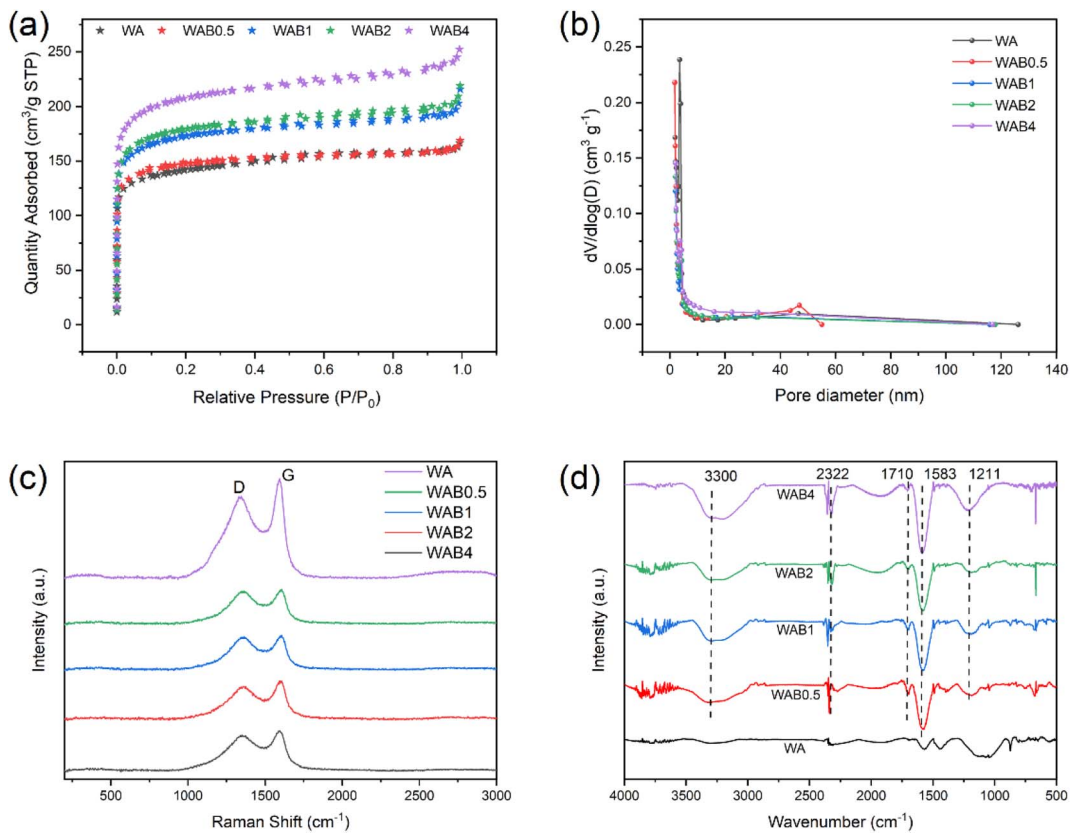

Fig. 2 (a) Nitrogen adsorption–desorption isotherms, (b) pore size distribution, (c) Raman spectra, (d) FTIR of WA, WAB0.5, WAB1, WAB2, and WAB4.

Table 1 BET surface area and pore volume of different biochars

Sample	Specific surface area ($m^2\ g^{-1}$)	Total pore volume ($cm^3\ g^{-1}$)	Micropore volume[a] ($cm^3\ g^{-1}$)	Micropore surface area ($m^2\ g^{-1}$)	Micropore percentage (%)	Average pore width (nm)
W	1.44	0.0069	0	0	0	19.15
WA	436.29	0.26	0.1971	378.5665	0.868	2.34
WAB0.5	446.39	0.26	0.2177	416.4498	0.933	2.29
WAB1	538.50	0.32	0.2535	496.4523	0.922	2.35
WAB2	552.92	0.33	0.2738	526.0977	0.951	2.37
WAB4	640.60	0.39	0.2970	574.2535	0.896	2.41

[a] The micropore volume and micropore surface area were calculated by *t*-plot.

stretching vibration absorption peak of C=O. The characteristic band at 1710 cm^{-1} belongs to the C=O stretching of ketones, aldehydes, and esters, which is the characteristic absorption peak of the lignin structure, demonstrating that the carbonized biochar still retains the lignin structure.[50] The broad band centered at 1583 cm^{-1} was due to stretching vibrations of C=O and C=C,[51,52] which increased significantly in modified biochar, indicating an improvement in the oxygen-containing functional groups. Compared with the pristine biochar, the C–B/B–O/C–O bond broad peak is slightly enhanced at 1211 cm^{-1} after boron incorporation, indicating the presence of hydroxyl-derived B–O deformation here. FTIR analysis revealed that the boric acid modification altered the structure of oxygen-containing functional groups of biochar, and the characteristic peaks were similar before and after the modification, indicating that the boric acid modification had little effect on the organic functional group types of biochar. However, it increased the stretching vibration of oxygen-containing groups such as hydroxyl groups in biochar, among which WAB4 was the most obvious.

The XPS test explored the carbon bonding state of the biochar surface (Table S3†). Fig. 3a shows the XPS survey spectra of unmodified WA and modified WAB4 with increased O content after modification. The C 1s of WA (Fig. 3b) can be deconvoluted into three peaks: 284.80, 286.3, and 289.49 eV, which were respectively assigned to the sp^2 C (63.21%), C–O (16.5%), and O–C=O (7.55%).[23,53] The sp^2 C content decreased while the –COOH content increased with the increase of the activation ratio. Similarly, the O 1s spectrum (Fig. 3c) of WA contains two distinct convolution peaks: 531.62 and 533.35 eV, which were respectively assigned to the C=O (5.43%) and –OH (5.44%).[54,55] WAB4 had the highest C=O and –OH content, implying that activation can increase the content of reactive groups. The aqueous boric acid solution produces water vapor during the pyrolysis process and oxidizes the carbon surface by generating mainly H_2, CO, and CO_2, so there is a small amount of CO and CO_2 in WAB4.[52] The two main peaks 192.14 eV and 190.63 eV in Fig. 3d are attributed to BCO_2 (0.51%) and BC_3 (0.12%), respectively.[56,57] The B1 content was consistent with the elemental analysis.

3.2. Screening for the best adsorption conditions

First, the modified biochar was prepared under different ratios of boric acid aqueous solutions, and then the prepared biochar (WA, WAB0.5, WAB1, WAB2, and WAB4) were adsorbed for four pesticides. It can be observed from Fig. 4a, that WA showed poor adsorption of pesticides, especially imidacloprid, and thiamethoxam. The poor adsorption of imidacloprid and thiamethoxam by WA may be because WA is unmodified, has a small specific surface area, small and few pores, and few adsorption sites available. Same as the molecular volume of imidacloprid and thiamethoxam is larger compared to tricyclazole and propiconazole, the small pores will affect the adsorption efficiency of large molecules.[58] The adsorption effect increased with the proportion of aqueous boric acid solution, with WAB4 exhibiting the highest adsorption effect on four pesticides. WAB4 contains electron-deficient B, and the vacant p-orbitals feature can act as Lewis acid sites to facilitate pesticide adsorption.[46] Meanwhile, WAB4 contains more pores, which are favorable for pore filling of pesticides. Then, the adsorption conditions of pesticides adsorbed by WAB4 were optimized, including the amount of WAB4, the selection of initial concentrations of four pesticides, and the adsorption time.

3.2.1. Selection of adsorbent dosage. The adsorption was performed by adding 2–20 mg (2, 5, 10, 15, and 20) of WAB4 in a mixed system of 10 mL of the four pesticides at an initial concentration of 5 mg L^{-1}. As can be seen from Fig. 4c, the removal efficiency of pesticides gradually increased with the increase of WAB4. The removal rate of all four pesticides reached more than 90% when the adsorbent dosage reached 1 g L^{-1}. Then, combining cost and resource saving considerations, firstly, walnut shells are domestic and agricultural waste, a renewable and green resource, and secondly, the one-step synthesis makes the preparation process simple and cost-saving. 1 g L^{-1} was chosen as the best adsorbent dosage in this experiment. According to the hydrophobic mechanism of action (Table S4†), the adsorption effect should be: propiconazole > tricyclazole > imidacloprid > thiamethoxam. However, the actual adsorption effect was: tricyclazole > propiconazole > imidacloprid > thiamethoxam, where the neonicotinoid insecticides imidacloprid and thiamethoxam were consistent with the hydrophobic effect, also demonstrating that there were other mechanisms of action besides hydrophobic effects to control the adsorption of pesticides by WAB4.[59]

3.2.2. Screening of the initial concentration of pesticides. Adsorption experiments were carried out on aqueous solutions of a mixture of four pesticides at initial concentrations of 0.1–

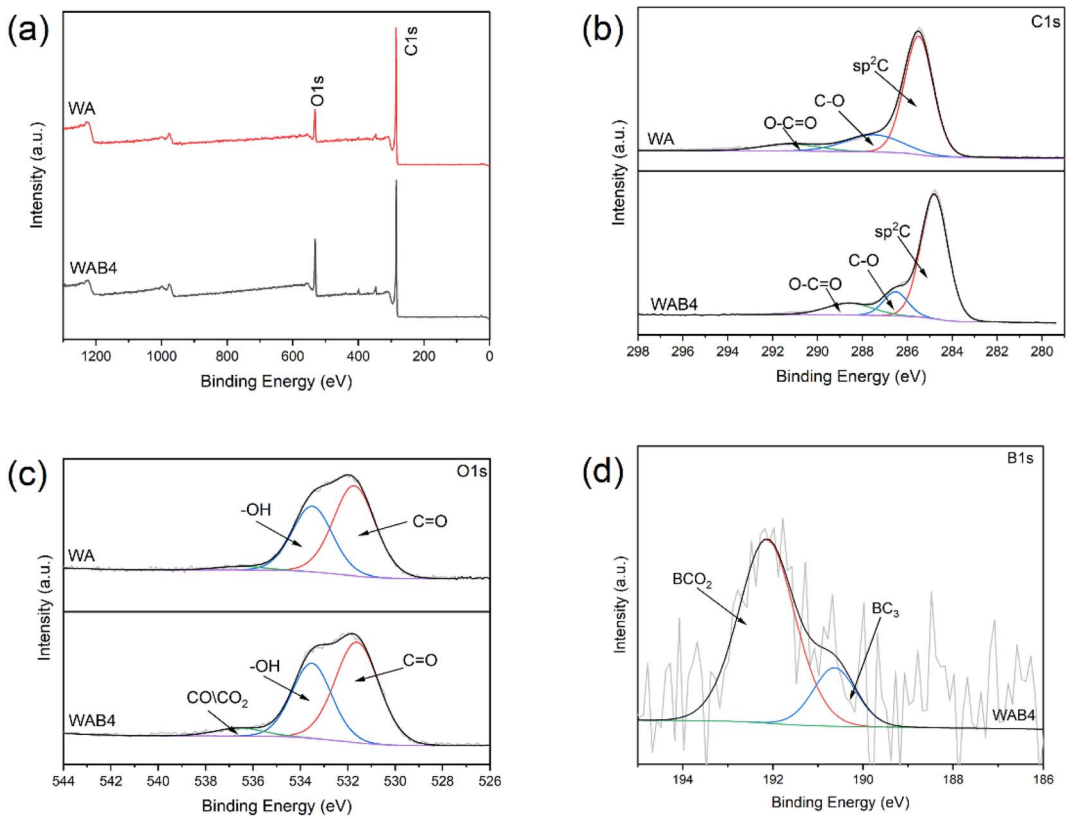

Fig. 3 (a) XPS survey spectra of WA and WA4; (b–d) high-resolution XPS spectra of C 1s, O 1s, and B 1s.

10 mg L^{-1} in 10 mL centrifuge tubes with 10 mg of adsorbent. The relationship between initial concentration and capacity is plotted in Fig. 4b, with tricyclazole, propiconazole, and imidacloprid showing a linear increase in adsorption capacity as the concentration increased. However, the adsorption capacity of thiamethoxam was significantly lower than the other three pesticides at 10 mg L^{-1}. This is because fixed doses of adsorbent do not provide sufficient adsorption sites, resulting in a gradual approach to the satiation of the adsorption capacity. Therefore, an initial concentration of 5 mg L^{-1} in the mixed aqueous solution was chosen as the optimum test dose.

3.2.3. Optimization of adsorption time. The adsorption time is one of the important factors affecting the adsorption effect. A 200 mL pesticide mixture was prepared at a concentration of 5 mg L^{-1}, and 10 mL was sampled at 0, 1, 2, 3, 5, 7, 10, 15, 20, and 30 min, respectively, and each point was repeated three times. Then 10 mg of WAB4 was added, vortex shaken for different times, and the supernatant was centrifuged to determine the concentration. The results are shown in Fig. 4d, tricyclazole, propiconazole, and imidacloprid reached adsorption equilibrium at 15 min, while thiamethoxam tended to equilibrium at 30 min. Therefore, the optimal adsorption time was selected as 30 min.

3.3. Effect of pH

Zeta potential is closely related to pH and was measured with ZS90 for all materials in aqueous solutions at pH 3–11. A concentration of 1 g L^{-1} was chosen for the materials and the results are shown in Fig. S4.† Where WA is the unmodified biochar, which is positively charged at pH < 5, the absolute value of the zeta potential is low, indicating that WA is less stable. The overall trend in zeta potential for the boric acid modified biochar was consistent, with all being negatively charged at pH 3–11, indicating that the boric acid modification increased the surface charge of the biochar. The smaller differences may be due to the different addition ratios of boric acid. At pH 3–11, WAB4 was negatively charged and at pH 7–11, the absolute value was larger and the system was more stable. The absolute value of the zeta potential increases with increasing pH due to the production of hydroxyl and carboxyl groups during the pyrolysis process.[60–62] As shown in Fig. 5a, the removal of all four pesticides was favorable at pH 7. The removal of imidacloprid and thiamethoxam was higher at pH 3. Compared with pH 7, imidacloprid and thiamethoxam undergo partial decomposition under alkaline conditions.[63] Tricyclazole and propiconazole maintained a high removal effect under all conditions and seemed to be independent of pH values,[3] indicating that the electrostatic effect was weak, whereas mechanisms such as hydrogen bonding, pore filling, and π–π interactions might be the main adsorption mechanisms for the above four pesticides.[41] However, except for the degradation of the pesticides themselves, the removal effects of all four pesticides were greater than 70% at pH 3–9, which proved that WAB4 has broad pH adaptability.

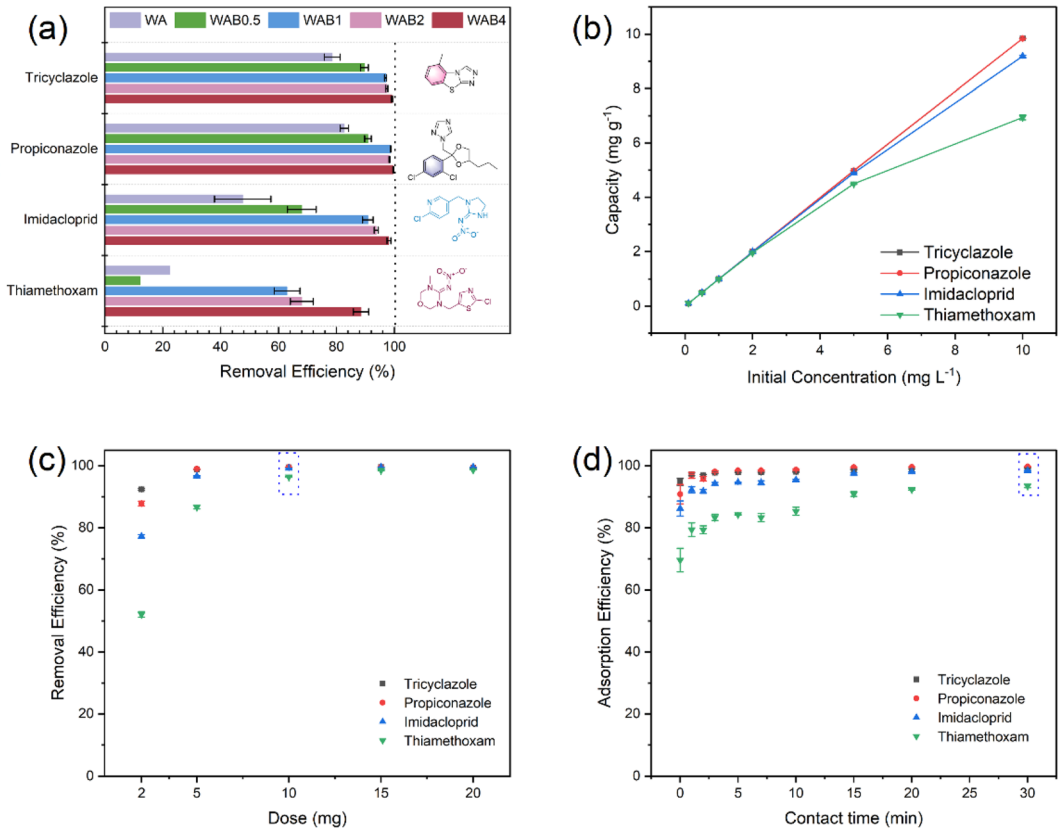

Fig. 4 (a) Adsorption optimization of modified biochar (WA, WAB0.5, WAB1, WAB2, and WAB4) (C_0 = 2 mg L^{-1}, pH = 7, T = 298 K); (b) initial concentrations of four pesticides (C_0 = 0.1–10 mg L^{-1}, pH = 7, T = 298 K); (c) optimization of adsorbent dosage (C_0 = 5 mg L^{-1}, adsorbent dosage = 0.2–2 g L^{-1}, pH = 7, T = 298 K); (d) optimization of adsorbent and pesticides contact time (C_0 = 5 mg L^{-1}, adsorbent dosage = 1 g L^{-1}, pH = 7, T = 298 K, time = 0–30 min).

Fig. 5d showed the removal of the four pesticides by recycling the biochar material five times. After 5 adsorption–desorption cycles, the removal efficiency can still reach 90%. The adsorption efficiency of tricyclazole, propiconazole, imidacloprid, and thiamethoxam was 97.6%, 98%, 96.2%, and 90.6% respectively. The adsorption efficiency of pesticides has decreased, probably because the cleaning material was not thorough and some pesticides were not desorption. These results suggest that WAB4 may be an efficient and economical adsorbent for pesticide removal from practical aqueous environments.

3.4. Adsorption kinetics

Fig. 6a–c shows the adsorption action of WAB4 for four pesticides at 5 mg L^{-1}. The adsorption increased rapidly within 10 min and then gradually reached equilibrium. Three kinetic models, the pseudo-first-order, pseudo-second-order, and Elovich kinetic models were used to simulate the adsorption process to understand the adsorption mechanism of WAB4 on four pesticides. The expressions of the three models are shown in eqn (S1)–(S3).† Table 2 shows the kinetic parameters and correlation coefficients, where the value of R^2 for the pseudo-second-order kinetic model (>0.9967) is greater than the value of the pseudo-first-order kinetic model.[64–66] Besides, the equilibrium quantity (q_e) estimated by the pseudo-second-order kinetic model is closer to the experimental values.

The intra-particle diffusion model (the formula is in eqn (S4)†) can be used to explore the adsorption rate controlling steps throughout the adsorption process.[67] At different stages of adsorption, the adsorption rate is controlled by different types of diffusion, where K_p is the slope of a straight line. The larger the value of K_p, the easier it is for the adsorbate to diffuse inside the adsorbent. C is the straight line intercept, which is related to the thickness of the boundary layer, the larger the C value, the greater the influence of the boundary layer, if $C = 0$, it indicates that intra-particle diffusion is the only rate control step, if $C \neq 0$, it indicates that the adsorption mechanism is more complex, intraparticle diffusion is not the only rate-controlling step.[68] The adsorption of each pesticide consists of three linear segments (Fig. 6d and Table 3). The intra-particle diffusion constant (K_p) values (Table 3) decrease in the following order $K_{p1} > K_{p2} > K_{p3}$ which indicates that internal diffusion is closely associated with the adsorption process. In the first stage of fitting, the slope is larger, indicating that its mass transfer rate is larger. This is because the concentration of pollutants in the solution in the early stage is relatively high, so the concentration gradient is relatively large, the mass transfer resistance is small, and the adsorption rate is large. In the second stage, the slope becomes

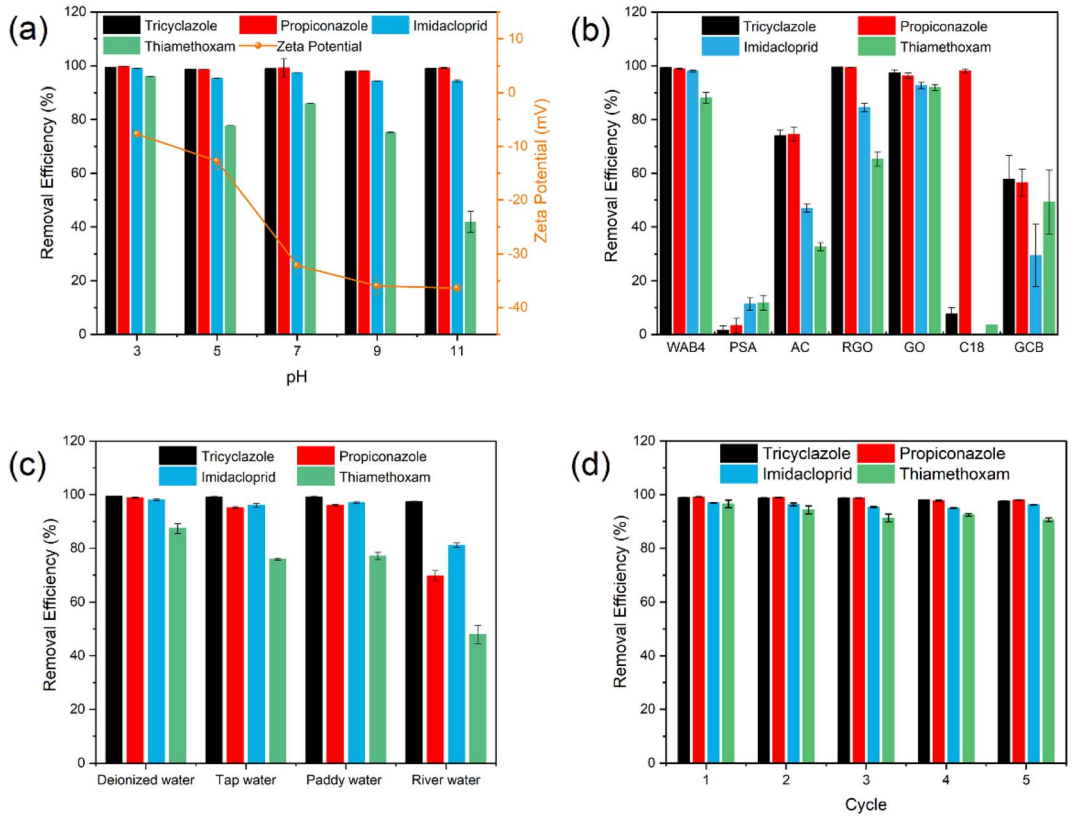

Fig. 5 (a) The effect of pH on adsorption performance and zeta potential of WAB4; (b) compared with common adsorbents (PSA, AC, RGO, GO, C18, and GCB); (c) adsorptive removal of pesticides by WAB4 in real water samples; (d) regeneration study for four pesticides removal onto the WAB4 (C_0 = 5 mg L^{-1}, adsorbent dosage = 1 g L^{-1}, pH = 7, T = 298 K).

smaller, because the concentration of pollutants decreases, the corresponding concentration gradient becomes smaller, the adsorption sites decrease, and the adsorption rate slows down. In the third stage, the adsorption gradually reached equilibrium. The trends in the adsorption of the four pesticides by WAB4 were consistent, while the fitted curves did not pass the origin, indicating that intra-particle diffusion is not the only rate control step for pesticide adsorption by WAB4.[64]

3.5. Adsorption isotherm

The Langmuir, Freundlich, and Temkin models (equations in ESI (S5)–(S7)†) were used to fit the sorption data. The Langmuir isotherm model is one of the commonly used adsorption isotherm models. It assumes that the adsorbent is uniformly adsorbed on the surface and that there are a uniform number of adsorption sites on the surface of the adsorbent material. All adsorption sites have the same energy, which is suitable for the monolayer adsorptions model.[49] The Freundlich isotherm model has a wide range of applications and is primarily used to fit the adsorption of multilayer heterogeneous surfaces and active sites with different energies. The Temkin isotherm model is mainly used for electrostatic interactions of adsorbents and adsorbates.[69,70]

Fig. 7a shows the fitted curves of the relationship between the equilibrium concentration (C_e) and the equilibrium adsorption amount (q_e) of tricyclazole at different temperatures. The adsorption of WAB4 on tricyclazole, propiconazole, and imidacloprid gradually increased with the increase of the initial concentration of pesticides. This is attributed to the concentration gradient driving force.[71] In addition, as the temperature increased from 25 °C to 45 °C, the adsorption capacity of tricyclazole, propiconazole, and imidacloprid increased. This is attributed to the fact that increased temperature increases the thermal movement of pesticides in the WAB4 pores, increasing the chance of collision. On the contrary, the adsorption capacity of thiamethoxam decreased with increasing temperature. The energy required for WAB4 to remain in the aqueous thiamethoxam solution for a longer period may increase with increasing temperature.[72] The model fit revealed that the correlation between the adsorption process of tricyclazole and the Freundlich (Fig. 7c) isotherm was better than that of the Langmuir (Fig. 7b) and Temkin (Fig. 7d) isotherm models. From the data (Table 4), it can be seen that the Freundlich isotherm model (R^2 > 0.99) was the best fit for the four pesticides. It is suggested that the adsorption of all four pesticides on WAB4 was multi-point non-homogeneous, which may be related to the heterogeneity of the adsorbent surface. In Table 4, $1/n$ between 0–1 means it is favorable (if $1/n = 0$ it is irreversible, if $1/n > 1$, it is unfavorable). The adsorption of imidacloprid on biocomposites prepared from peanut shells and polypyrrole conforms to the Freundlich isotherm model, likewise.[73]

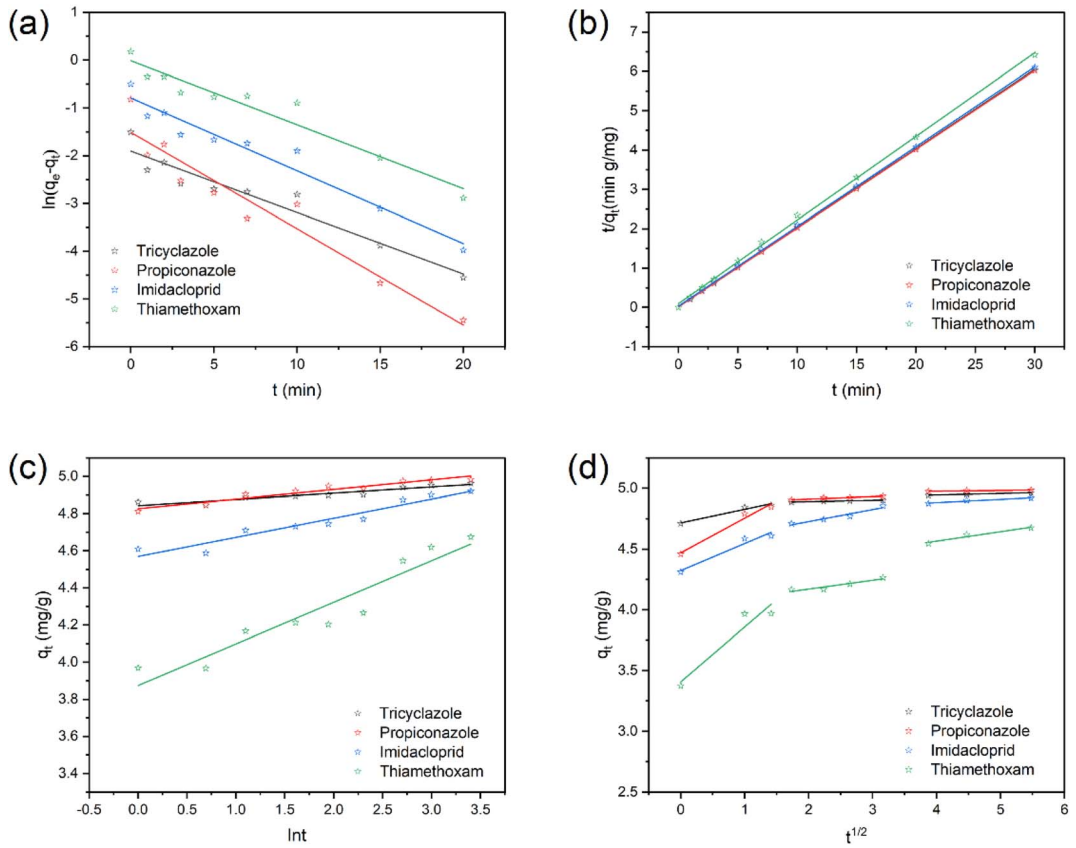

Fig. 6 The kinetic models of four pesticides: (a) pseudo-first-order kinetic model; (b) pseudo-second-order kinetic model; (c) Elovich model; (d) intra-particle diffusion model (C_0 = 5 mg L^{-1}, adsorbent dosage = 1 g L^{-1}, pH = 7, T = 298 K, time = 0–30 min).

According to the fitting results of the Langmuir model, the adsorption capacities of the four pesticides were 171.67 mg g^{-1} (tricyclazole), 112.27 mg g^{-1} (propiconazole), 156.40 mg g^{-1} (imidacloprid), and 144.63 mg g^{-1} (thiamethoxam), respectively. The maximum adsorption capacities fitted by the Langmuir model were very close to the experimental data.

3.6. Adsorption thermodynamics

Thermodynamic parameters can be used as another indicator to speculate a reasonable adsorption mechanism. Thermodynamic parameters include standard Gibbs free energy change (ΔG^0), standard enthalpy change (ΔH^0), and standard entropy change (ΔS^0), the equation is as follows:

$$\Delta G^0 = -RT\ln K_0$$

$$\Delta G^0 = \Delta H - T\Delta S^0$$

$$\ln K_0 = \frac{-\Delta H}{R} \times \frac{1}{T} + \frac{\Delta S}{R}$$

where R (8.314 J mol^{-1} K^{-1}) is the universal gas constant, T (K) is the absolute temperature, and K_0 (dimensionless) is the equilibrium constant.[42]

The thermodynamic parameters (Table S5†) of adsorption were calculated from the van't Hoff plots (Fig. S2†) and the above equations. The ΔG of the adsorption process was negative at all the selected temperatures, indicating that the adsorption process of the materials on the pesticides was spontaneous. The absolute values of ΔG increased with increasing temperature for

Table 2 Parameters of kinetic models for four pesticides adsorption on WAB4

Kinetic model	Pseudo-first-order			Pseudo-second-order		
Pesticides	q_e (mg kg^{-1})	k_1 (min^{-1})	R^2	q_e (mg kg^{-1})	k_2 (g mg^{-1} min^{-1})	R^2
Tricyclazole	0.1490	0.12865	0.9145	4.96	3.668	0.9998
Propiconazole	0.2207	0.20184	0.9128	4.99	3.836	0.9999
Imidacloprid	0.4537	0.15251	0.9426	4.93	1.295	0.9998
Thiamethoxam	0.9875	0.13389	0.9278	4.70	0.4815	0.9989

Table 3 Intra-particle diffusion parameters for four pesticides adsorption on WAB4

Pesticides	K_{p1} (mg g^{-1} min^{-1})	C (mg g^{-1})	R^2	K_{p2} (mg g^{-1} min^{-1})	C (mg g^{-1})	R^2	K_{p3} (mg g^{-1} min^{-1})	C (mg g^{-1})	R^2
Tricyclazole	0.113	4.72	0.887	0.0098	4.870	0.958	0.01106	4.900	0.959
Propiconazole	0.267	4.50	0.852	0.0162	4.880	0.686	0.00522	4.950	0.906
Imidacloprid	0.176	4.39	0.530	0.0673	4.595	0.948	0.02310	4.797	0.758
Thiamethoxam	0.491	3.41	0.834	0.0738	4.017	0.818	0.06830	4.310	0.787

the adsorption processes of tricyclazole, propiconazole, and imidacloprid while both ΔH and ΔS were positive, indicating that increasing the temperature favors the adsorption process and that the adsorption is voluntary, endothermic and disorder-increasing.[74] The adsorption process of thiamethoxam decreases with the increase of temperature, and the absolute value of ΔG decreases, while ΔH and ΔS are both negative values, the adsorption is spontaneous, exothermic, and disordered. The ΔG of all four pesticides was in the range of -20 to 0 kJ mol^{-1}, so the adsorption was a physical adsorption process.[75] The positive values of ΔH and ΔS for tricyclazole, propiconazole, and imidacloprid indicate that hydrophobic interaction is the main force of adsorption, while the negative values of ΔH and ΔS for thiamethoxam indicate that hydrogen bonding is the main forces of adsorption.[76,77]

3.7. Possible adsorption mechanism

According to the above characterization data and adsorption experiments, the adsorption process of WAB4 on the four pesticide contaminants is mainly physical adsorption. The specific surface area and pore size analysis showed that WAB4 has a high specific surface area with abundant adsorption sites, the average pore size is 2.41 nm, and the volume of micropores is 89.6%, which is conducive to the diffusion and pore filling of pesticide pollutants.[44] The adsorption characteristics of tricyclazole and propiconazole at different initial pH conditions showed that the adsorption of tricyclazole and propiconazole was unaffected by pH, and the adsorption amounts of the other three were similar at pH 3 and 7, illustrating that the electrostatic interaction was weak. According to the FTIR diagram of WAB4 before and after adsorption in Fig. S3,† four major

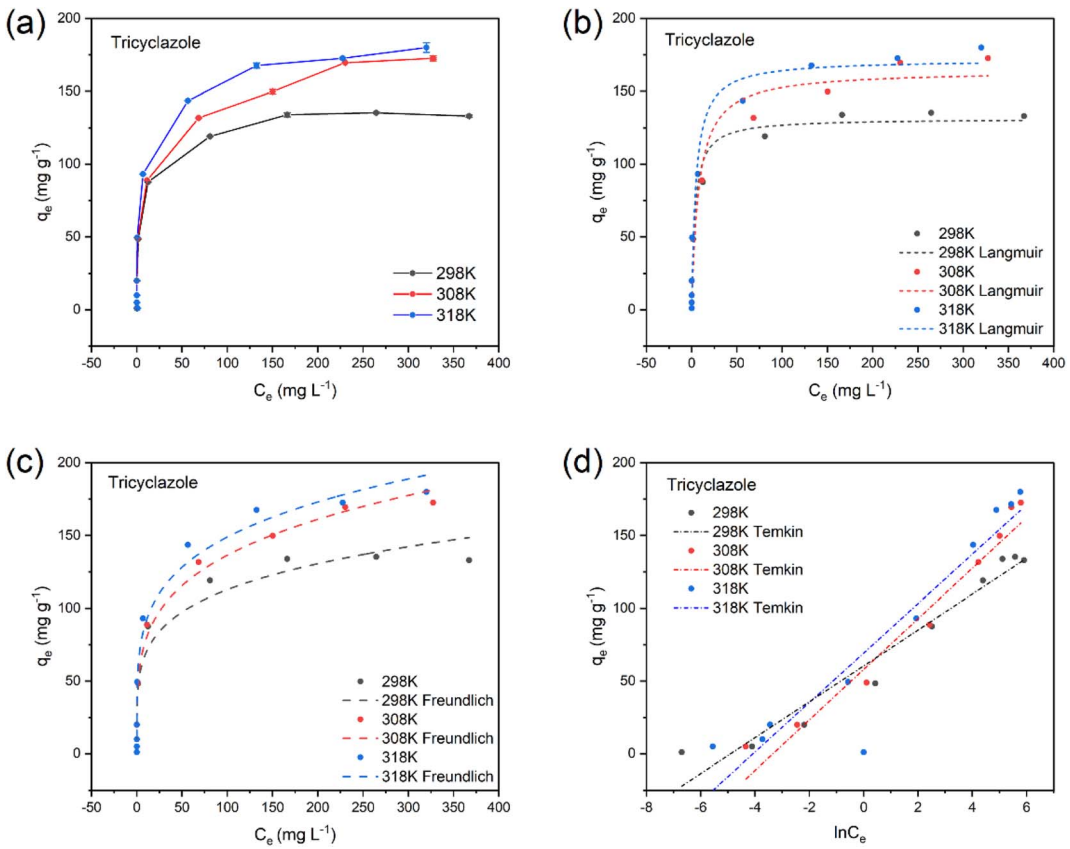

Fig. 7 (a) Adsorption isotherms of tricyclazole; (b) Langmuir model; (c) Freundlich model; (d) Temkin model at 298 K, 308 K, and 318 K. ($C_0 = 1$–500 mg L^{-1}, adsorbent dose = 1 g L^{-1}, pH = 7, T = 298 K, 308 K, 318 K).

Table 4 Results of isotherm models for four pesticides adsorption on WAB4

		Langmuir			Freundlich			Temkin		
Pesticides	T	q_m (mg g^{-1})	K_l (L mg^{-1})	R^2	K_f (L mg^{-1})	$1/n$	R^2	B (J mol^{-1})	K_T (L mg^{-1})	R^2
Tricyclazole	298	131.34	0.27536	0.97	42.5134	0.212	0.97	12.33	134.2136	0.954
	308	164.20	0.13082	0.96	45.1489	0.240	0.99	17.37	28.2422	0.881
	318	171.67	0.2162	0.96	54.9381	0.216	0.98	16.99	58.8358	0.86
Propiconazole	298	108.27	0.13843	0.94	30.1900	0.296	0.99	8.06	383.4220	0.857
	308	103.20	0.37827	0.93	34.7500	0.295	0.99	9.58	301.8144	0.867
	318	112.27	0.49121	0.95	40.7000	2.882	0.98	11.69	149.8163	0.95
Imidacloprid	298	136.08	0.16384	0.97	40.3977	0.224	0.97	12.42	125.8315	0.934
	308	148.35	0.16394	0.96	42.9503	0.230	0.96	14.42	79.4536	0.956
	318	156.40	0.1101	0.96	39.9944	0.251	0.98	14.35	89.5479	0.919
Thiamethoxam	298	137.46	0.04194	0.96	24.5707	0.307	0.99	11.27	69.9346	0.874
	308	132.38	0.04144	0.96	23.6078	0.305	0.98	11.18	53.2954	0.876
	318	127.84	0.04925	0.97	23.8303	0.301	0.98	11.39	40.3302	0.877

differences can be found. It is noteworthy that the peak used for –OH tensile vibration at 3300 cm^{-1} is significantly reduced. After adsorption, the tensile vibration of wave number 2322 cm^{-1} weakens, indicating that C≡C or C≡N participates in adsorption. The contaminant contains a benzene ring, which can form π–π interaction with the sp^2 hybrid material surface.[78] A similar pattern distinguished at peak 1583 cm^{-1} was assigned to (C=O, COOH stretching) which was diminished, indicating that C=O was involved in the adsorption of pesticides. In addition, the stretching vibration of the carbonyl group weakened at 1211 cm^{-1}, indicating that oxygen-containing functional groups (carboxyl and hydroxyl groups) may be involved in the adsorption of pesticides on the surface of biochar. Thermodynamic results indicate that hydrophobic interactions play a dominant role in the adsorption of tricyclazole, propiconazole and imidacloprid, and hydrogen bonding plays a dominant role in the adsorption of thiamethoxam. In addition, the abundant carbon chemical bonds and the larger conjugation system in WAB4 can form strong π–π interactions with the π-rich aromatic and triazine/pyrimidine/pyridine rings in pesticides. For example, tricyclazole has a strong aromatic character and planar geometry, lacks polar functional groups, and interaction with WAB4 may occur more through the π-electron of the aromatic ring and the lone electron pair of the S atom.[79]

In summary, the adsorption of thiamethoxam is dominated by hydrogen bonding and hydrophobic interactions, while imidacloprid, tricyclazole, and propiconazole are dominated by hydrophobic interactions. Based on the above analysis, it is worth noting that π–π interactions and pore filling should also be auxiliary forces for adsorption (Fig. 8).

3.8. Comparison with commercial material

A mixture of four pesticides (5 mg L^{-1}) in an aqueous solution was adsorbed with different materials (1 g L^{-1}) for 30 min at 25 °C. After centrifugation, the pesticide concentration in the supernatant was measured. The adsorption efficiency was calculated from the concentration results. According to Fig. 5b,

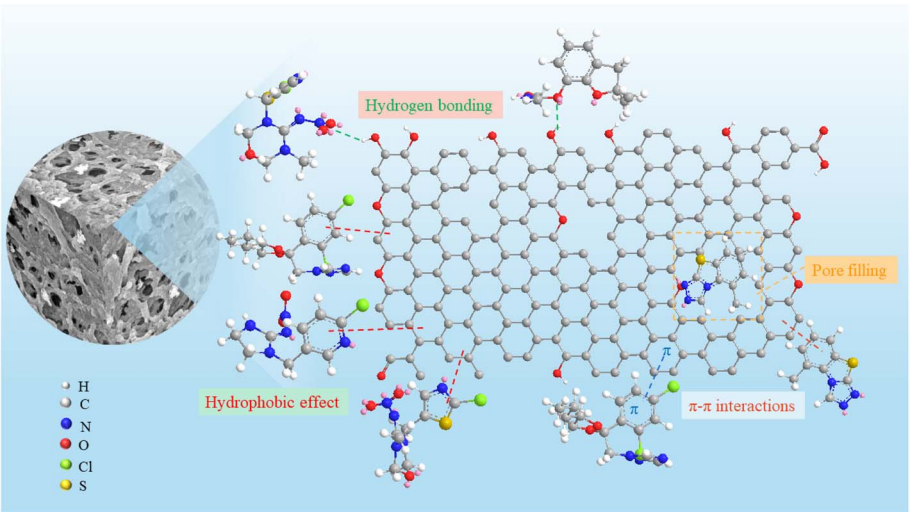

Fig. 8 Possible adsorption mechanism of WAB4 for four pesticides (tricyclazole, propiconazole, imidacloprid, and thiamethoxam).

compared with the other commonly used adsorbents, WAB4 had a higher removal rate of four pesticides. PSA (primary secondary amine) and C18 (octadecyl silane) have poor adsorption of four pesticides, with removal rates below 20%. The adsorption efficiency of AC (activated carbon) and GCB (graphitized carbon black) were low for four pesticides, and less than 50% for imidacloprid and thiamethoxam. RGO (reduced graphene oxide) was not effective in removing all pesticides and have an adsorption efficiency of 60–80% for imidacloprid and thiamethoxam. The GO (graphene oxide) adsorption efficiency was comparable to that of WAB4. Considering the cost, WAB4 is competitive in practical applications.

3.9. Performance in real water

To test the general applicability of the adsorbent, the removal efficiency of WAB4 in real water bodies should be tested. Tap water from the laboratory (Beijing, China), paddy water from Huailai County, Bengbu City (Anhui, China), and river water from the Nansha River (Beijing, China). Each water sample was taken in 10 mL, spiked with 5 mg L^{-1} of the four pesticides and 1 g L^{-1} WAB4, and adsorbed at 25 °C for 30 min. The supernatant was collected by centrifugation, filtered through a 0.22 μm nylon filter, and analyzed by HPLC-MS/MS. Each experiment was performed in triplicate and the data obtained were averaged. Inorganic salts are commonly found in natural water, so four water samples were tested for their physicochemical properties, as shown in Table S6.† Fig. 5c shows the removal results of four pesticides in deionized water, tap water, paddy water, and river water. The results showed that deionized water, tap water, and paddy water had very similar removal effects, except thiamethoxam. In addition, the removal efficiency of river water decreased slightly. This may be caused by the presence of natural organic matter in the river water, which affects the adsorption.[80] The hydrophobic use of thiamethoxam was the weakest in the system, and thiamethoxam was at a disadvantage when the four pesticides competed for adsorption, resulting in a lower adsorption efficiency of thiamethoxam than the other three pesticides. Meanwhile, the sodium and chloride ion content of river water was significantly higher than that of pure water, tap water, and rice paddy water. Because of the increased ion content, competitive adsorption with pesticides occurred, which ultimately affected the adsorption effect of pesticides in river water.[81] However, the removal efficiency of all four pesticides in paddy water was maintained at over 70%, so WAB4 can be applied to the removal of pesticides in the real environment.

3.10. Environmental safety evaluation

Considering the future potential of WAB4 in practical applications, a range of material concentrations were set up for toxicity examination. The experiment's results are shown in Table S7,† where WAB4 was observed to be dispersed at the bottom of the beaker and *Daphnia magna* could molt and swim in the water normally. No acute toxicity and no significant inhibition were observed in *Daphnia magna* exposed to WAB4 for 24 h and 48 h.

4. Conclusions

In this study, modified biochar prepared from raw walnut shells and boric acid solution was successfully prepared by a one-step pyrolysis method. The method is based on the direct synthesis of biochar in a one-step process in a muffle furnace without the need for nitrogen protection, a simple preparation process, and low experimental costs. WAB4 is relatively competitive with the reported adsorbents. The experimental results indicated that the adsorption process was more consistent with the pseudo-second-order kinetic and Freundlich isotherm model, demonstrating that WAB4 is a heterogeneous sorbent. The adsorption of pesticides by WAB4 is based on physical adsorption, according to the results of adsorption thermodynamics. The adsorption capacity of WAB4 to tricyclazole, propiconazole, imidacloprid, and thiamethoxam up to 171.67, 112.27, 156.40, and 137.46 mg g^{-1}, respectively. Further exploration of the adsorption mechanism suggests that pore filling, hydrogen bonding, hydrophobic interactions, and π–π interactions may be the main driving forces for the adsorption of pesticides by WAB4. In addition, WAB4 exhibited a fast removal rate, wide pH adaptability (pH 3–9), renewability, and biosafety, which makes it a promising and environmentally friendly adsorbent providing an important reference for the removal of pollution.

Author contributions

Niannian Cao: investigation, writing-original draft. Jiawen Ji: formal analysis. Changsheng Li: investigation. Meng Yuan: data curation. Xuanjun Guo: investigation. Xingxing Zong: validation. Liqin Li: methodology. Yongqing Ma: writing-review & editing. Chen Wang: funding acquisition. Sen Pang: conceptualization, project administration.

Conflicts of interest

There are no conflicts to declare.

References

1 A. M. Carey, K. G. Scheckel, E. Lombi, M. Newville, Y. Choi, G. J. Norton, J. M. Charnock, J. Feldmann, A. H. Price and A. A. Meharg, *Plant Physiol.*, 2010, **152**, 309–319.
2 L. Padovani, E. Capri, C. Padovani, E. Puglisi and M. Trevisan, *Chemosphere*, 2006, **62**, 303–314.
3 M. Garcia-Jaramillo, L. Cox, H. E. Knicker, J. Cornejo, K. A. Spokas and M. C. Hermosin, *J. Hazard. Mater.*, 2015, **286**, 581–588.
4 M. S. Krieger, W. L. Cook and L. M. Kennard, *J. Agric. Food Chem.*, 2000, **48**, 2178–2183.
5 D. G. Bottrell and K. G. Schoenly, *J. Asia-Pac. Entomol.*, 2012, **15**, 122–140.
6 Z. Fu, F. Han, K. Huang, J. Zhang, J. G. Qin, L. Chen and E. Li, *Sci. Total Environ.*, 2022, **830**, 154799.
7 C. A. Morrissey, P. Mineau, J. H. Devries, F. Sanchez-Bayo, M. Liess, M. C. Cavallaro and K. Liber, *Environ. Int.*, 2015, **74**, 291–303.

8 G. Rodriguez-Castillo, M. Molina-Rodriguez, J. C. Cambronero-Heinrichs, J. P. Quiros-Fournier, V. Lizano-Fallas, C. Jimenez-Rojas, M. Masis-Mora, V. Castro-Gutierrez, I. Mata-Araya and C. E. Rodriguez-Rodriguez, *Chemosphere*, 2019, **235**, 1097–1106.
9 Q. Zhang, Z. Li, C. H. Chang, J. L. Lou, M. R. Zhao and C. Lu, *Environ. Pollut.*, 2018, **236**, 71–81.
10 W. A. Battaglin, M. W. Sandstrom, K. M. Kuivila, D. W. Kolpin and M. T. Meyer, *Water, Air, Soil Pollut.*, 2011, **218**, 307–322.
11 G. Liu, L. Li, X. Huang, S. Zheng, D. Xu, X. Xu, Y. Zhang and H. Lin, *Microporous Mesoporous Mater.*, 2018, **270**, 258–264.
12 E. D. Tsochatzis, R. Tzimou-Tsitouridou, U. Menkissoglu-Spiroudi, D. G. Karpouzas and D. Katsantonis, *Chemosphere*, 2013, **91**, 1049–1057.
13 L. Cox, M. C. Fernandes, A. Zsolnay, M. C. Hermosin and J. Cornejo, *J. Agric. Food Chem.*, 2004, **52**, 5635–5642.
14 C. Ju, X. Li, S. He, L. Shi, S. Yu, F. Wang, S. Xu, D. Cao, H. Fang and Y. Yu, *J. Agric. Food Chem.*, 2020, **68**, 15381–15389.
15 X. Pan, Y. Cheng, F. Dong, N. Liu, J. Xu, X. Liu, X. Wu and Y. Zheng, *J. Hazard. Mater.*, 2018, **359**, 194–202.
16 L. Qiu, K. Jia, L. Huang, X. Liao, X. Guo and H. Lu, *Chemosphere*, 2019, **232**, 171–179.
17 Y. Cheng, B. Wang, J. Shen, P. Yan, J. Kang, W. Wang, L. Bi, X. Zhu, Y. Li, S. Wang, L. Shen and Z. Chen, *J. Hazard. Mater.*, 2022, **432**, 128757.
18 C. Zhou, C. Lai, D. Huang, G. Zeng, C. Zhang, M. Cheng, L. Hu, J. Wan, W. Xiong, M. Wen, X. Wen and L. Qin, *Appl. Catal., B*, 2018, **220**, 202–210.
19 Y. Li, F. Wang, Y. Miao, Y. Mai, H. Li, X. Chen and J. Chen, *Bioresour. Technol.*, 2020, **307**, 123165.
20 N. Zhou, H. Chen, J. Xi, D. Yao, Z. Zhou, Y. Tian and X. Lu, *Bioresour. Technol.*, 2017, **232**, 204–210.
21 A. Bogusz, P. Oleszczuk and R. Dobrowolski, *Bioresour. Technol.*, 2015, **196**, 540–549.
22 S. Kant Bhatia, A. K. Palai, A. Kumar, R. Kant Bhatia, A. Kumar Patel, V. Kumar Thakur and Y. H. Yang, *Bioresour. Technol.*, 2021, **340**, 125644.
23 X. Zhang, D. D. Gang, J. Zhang, X. Lei, Q. Lian, W. E. Holmes, M. E. Zappi and H. Yao, *J. Hazard. Mater.*, 2022, **424**, 127333.
24 M. Yuan, C. Li, B. Zhang, J. Wang, J. Zhu, J. Ji and Y. Ma, *Chemosphere*, 2021, **280**, 130877.
25 B. Liu, W. Guo, H. Wang, Q. Si, Q. Zhao, H. Luo and N. Ren, *Chem. Eng. J.*, 2020, **396**, 125119.
26 G. Liu, L. Li, D. Xu, X. Huang, X. Xu, S. Zheng, Y. Zhang and H. Lin, *Carbohydr. Polym.*, 2017, **175**, 584–591.
27 N. Singh, *J. Agric. Food Chem.*, 2002, **50**, 6434–6439.
28 M. R. Miladinović, M. V. Zdujić, D. N. Veljović, J. B. Krstić, I. B. Banković-Ilić, V. B. Veljković and O. S. Stamenković, *Renewable Energy*, 2020, **147**, 1033–1043.
29 F. Hemmati, S. M. Jafari, M. Kashaninejad and M. Barani Motlagh, *Int. J. Biol. Macromol.*, 2018, **120**, 1216–1224.
30 S. Qin, H. Fan, L. Jia, Y. Jin, Z. Li and B. Fan, *Energy Fuels*, 2022, **36**, 3184–3200.
31 A. Jahanban-Esfahlan, R. Jahanban-Esfahlan, M. Tabibiazar, L. Roufegarinejad and R. Amarowicz, *RSC Adv.*, 2020, **10**, 7026–7047.
32 S. Saadat, A. Karimi-Jashni and M. M. Doroodmand, *J. Environ. Chem. Eng.*, 2014, **2**, 2059–2067.
33 X. Geng, S. Lv, J. Yang, S. Cui and Z. Zhao, *J. Environ. Manage.*, 2021, **280**, 111749.
34 X. Zhang, X. Xia, H. Li, B. Zhu and J. Dong, *Environ. Sci. Technol.*, 2015, **49**, 10127–10135.
35 Organization for Economic Cooperation and Development (OECD), *OECD Guideline for Testing of Chemicals; Daphnia sp., Acute Immobilisation Test*, 2004.
36 J. Hou, Y. Zhou, C. Wang, S. Li and X. Wang, *Environ. Sci. Technol.*, 2017, **51**, 12868–12878.
37 M. Yuan, C. S. Li, B. J. Zhang, J. L. Wang, J. H. Zhu, J. W. Ji and Y. Q. Ma, *Chemosphere*, 2021, **280**, 130877.
38 S. Balci, N. A. Sezgi and E. Eren, *Ind. Eng. Chem. Res.*, 2012, **51**, 11091–11096.
39 H. Li, X. Dong, E. B. da Silva, L. M. de Oliveira, Y. Chen and L. Q. Ma, *Chemosphere*, 2017, **178**, 466–478.
40 S. Ye, G. Zeng, X. Tan, H. Wu, J. Liang, B. Song, N. Tang, P. Zhang, Y. Yang, Q. Chen and X. Li, *Appl. Catal., B*, 2020, **269**, 118850.
41 J. Xu, Y. Zhang, B. Li, S. Fan, H. Xu and D. X. Guan, *Chemosphere*, 2022, **296**, 133981.
42 D. Jiang, J. Yang and D. Wang, *Langmuir*, 2020, **36**, 3141–3148.
43 J. Wan, L. Liu, K. S. Ayub, W. Zhang, G. Shen, S. Hu and X. Qian, *Fuel*, 2020, **269**, 117142.
44 I. Kozyatnyk, P. Oesterle, C. Wurzer, O. Masek and S. Jansson, *Bioresour. Technol.*, 2021, **340**, 125561.
45 L. Yang, D. Wu, T. Wang and D. Jia, *ACS Appl. Mater. Interfaces*, 2020, **12**, 18692–18704.
46 F. Ye, Y. Shi, W. Sun, K. F. Pang, M. J. Pu, L. H. Yang and H. M. Huang, *Chem. Eng. J.*, 2023, **454**, 140148.
47 J. Yu, L. Sun, C. Berrueco, B. Fidalgo, N. Paterson and M. Millan, *J. Anal. Appl. Pyrolysis*, 2018, **130**, 127–134.
48 J. Xu, J. Liu, P. Ling, X. Zhang, K. Xu, L. He, Y. Wang, S. Su, S. Hu and J. Xiang, *Energy*, 2020, **202**, 117644.
49 Q. Yin, Y. Nie, Y. Han, R. Wang and Z. Zhao, *Langmuir*, 2022, **38**, 1833–1844.
50 P. J. M. Suhas and M. M. L. Carrott, *Bioresour. Technol.*, 2007, **98**, 2301–2312.
51 B. Chen, D. Zhou and L. Zhu, *Environ. Sci. Technol.*, 2008, **42**, 5137–5143.
52 G. de la Puente, J. J. Pis, J. A. Menéndez and P. Grange, *J. Anal. Appl. Pyrolysis*, 1997, **43**, 125–138.
53 H. Chen, Y. Gao, A. El-Naggar, N. K. Niazi, C. Sun, S. M. Shaheen, D. Hou, X. Yang, Z. Tang, Z. Liu, H. Hou, W. Chen, J. Rinklebe, M. Pohorely and H. Wang, *J. Hazard. Mater.*, 2022, **425**, 127971.
54 W. Chen, H. Yang, Y. Chen, K. Li, M. Xia and H. Chen, *Environ. Sci. Technol.*, 2018, **52**, 9514–9521.
55 Y. C. G. Kwan, G. M. Ng and C. H. A. Huan, *Thin Solid Films*, 2015, **590**, 40–48.
56 Y. Wang, C. Wang, Y. Wang, H. Liu and Z. Huang, *ACS Appl. Mater. Interfaces*, 2016, **8**, 18860–18866.

57 J. Han, L. L. Zhang, S. Lee, J. Oh, K.-S. Lee, J. R. Potts, J. Ji, X. Zhao, R. S. Ruoff and S. Park, *ACS Nano*, 2013, **7**, 19–26.
58 M. F. Tennant and D. W. Mazyck, *Carbon*, 2007, **45**, 858–864.
59 W. Chen, L. Duan and D. Zhu, *Environ. Sci. Technol.*, 2007, **41**, 8295–8300.
60 J. H. Yuan, R. K. Xu and H. Zhang, *Bioresour. Technol.*, 2011, **102**, 3488–3497.
61 R. K. Xu, S. C. Xiao, J. H. Yuan and A. Z. Zhao, *Bioresour. Technol.*, 2011, **102**, 10293–10298.
62 A. Mandal, N. Singh and T. J. Purakayastha, *Sci. Total Environ.*, 2017, **577**, 376–385.
63 Y. Yang, X. Ma, C. Yang, Y. Wang, J. Cheng, J. Zhao, X. Dong and Q. Zhang, *Chem. Eng. J.*, 2022, **430**, 132999.
64 Q. Mo, X. Yang, J. Wang, H. Xu, W. Li, Q. Fan, S. Gao, W. Yang, C. Gao, D. Liao, Y. Li and Y. Zhang, *Environ. Pollut.*, 2021, **291**, 118120.
65 V. Vimal, M. Patel and D. Mohan, *RSC Adv.*, 2019, **9**, 26338–26350.
66 S. S. Mayakaduwa, I. Herath, Y. S. Ok, D. Mohan and M. Vithanage, *Environ. Sci. Pollut. Res. Int.*, 2017, **24**, 22755–22763.
67 J. Zhu, S. Xiang, B. Zhang, J. Wang, C. Li, C. Pan, Y. Xu and Y. Ma, *J. Environ. Chem. Eng.*, 2022, **10**, 107724.
68 M. Haris, M. Usman, F. Su, W. Lei, A. Saleem, Y. Hamid, J. Guo and Y. Li, *Chem. Eng. J.*, 2022, **434**, 134842.
69 C. X. Yang, Q. Zhu, W. P. Dong, Y. Q. Fan and W. L. Wang, *Langmuir*, 2021, **37**, 9253–9263.
70 C. Li, N. Zhang, J. Chen, J. Ji, X. Liu, J. Wang, J. Zhu and Y. Ma, *Environ. Pollut.*, 2019, **255**, 113150.
71 J. H. Qu, Y. H. Yuan, Q. J. Meng, G. S. Zhang, F. X. Deng, L. Wang, Y. Tao, Z. Jiang and Y. Zhang, *J. Hazard. Mater.*, 2020, **400**, 123142.
72 R. R. V. Hemavathy, P. S. Kumar, S. Suganya, V. Swetha and S. J. Varjani, *Bioresour. Technol.*, 2019, **281**, 1–9.
73 F. Ishtiaq, H. N. Bhatti, A. Khan, M. Iqbal and A. Kausar, *Int. J. Biol. Macromol.*, 2020, **147**, 217–232.
74 Y. Ma, S. Chen, Y. Qi, L. Yang, L. Wu, L. He, P. Li, X. Qi, F. Gao, Y. Ding and Z. Zhang, *Chemosphere*, 2022, **291**, 132707.
75 Z. Gu, M. Gao, Z. Luo, L. Lu, Y. Ye and Y. Liu, *Appl. Surf. Sci.*, 2014, **290**, 107–115.
76 C. M. G. C. Renard, A. A. Watrelot and C. Le Bourvellec, *Trends Food Sci. Technol.*, 2017, **60**, 43–51.
77 P. D. Ross and S. Subramanian, *Biochemistry*, 1981, **20**, 3096–3102.
78 B. Zhang, J. Yu, C. Li, J. Wang, J. Zhu, Y. Ma, C. Yu and L. Duan, *Food Chem.*, 2022, **375**, 131899.
79 S. Azarkan, A. Pena, K. Draoui and C. Ignacio Sainz-Diaz, *Appl. Clay Sci.*, 2016, **123**, 37–46.
80 B. Wang, Y. Yang, Y. Lu, W. Wang, Q. Wang, X. Dong and J. Zhao, *Sci. Total Environ.*, 2020, **710**, 135512.
81 S. Z. Li, Z. H. Zhang, C. Zhang, Y. T. He, X. H. Yi, Z. G. Chen, M. A. Hassaan, A. El Nemr and M. Z. Huang, *Environ. Sci. Pollut. Res.*, 2022, **30**, 29143–29153.